Chinese Journal of
POLYMER SCIENCE

RESEARCH ARTICLE

https://doi.org/10.1007/s10118-026-3644-3
Chinese J. Polym. Sci. **2026**, *44*, 2269–2281

Soft-segment-engineered Self-healing Polyurethane for High-performance Electrorheological Elastomers and Capacitive Sensors

Yan-Bo Yang[a], Yao Wan[a], Zi-Xuan Zhang[a], Zhen-Jie Zhao[a*], Yong-Ri Liang[a], Hyoung Jin Choi[b], and Ying-Dan Liu[a*]

[a] *Center for Advanced Structural Materials, State Key Lab of Metastable Materials Science and Technology, and College of Materials Science and Engineering, Yanshan University, Qinhuangdao 066004, China*
[b] *Department of Polymer Science and Engineering, Inha University, Incheon 22212, Korea*

Electronic Supplementary Information

Abstract Polyurethane (PU) holds promise as a matrix for electrorheological elastomers (EREs) because of its excellent mechanical properties; however, its high modulus often limits electrorheological (ER) efficiency. This study addresses this by tailoring the soft-segment architecture of PU to adjust its mechanical and dielectric properties, thus improving the ER response of the PU-based ERE. Dynamic covalent bonds have also been introduced to enable self-healing. Using poly(propylene glycol) (PPG), poly(tetramethylene glycol) (PTMG), and polycaprolactone (PCL) as the soft segments, we fabricated EREs with 20 wt% TiO_2. The resulting PPG-ERE exhibited an outstanding ER effect of 229.4% at 3 kV/mm, along with a high stretchability (1835% elongation) and tensile strength of 3.6 MPa. PTMG-ERE has the highest storage modulus of 1.43 MPa at 3 kV/mm and a relatively high tensile strength of up to 6.5 MPa, which is attributed to enhanced hydrogen bonding interactions among the regular PTMG segments. The PCL-ERE with the highest Young's modulus resulted in the lowest ER efficiency of 48% because of its high crystallization tendency. The PPG-ERE also demonstrated efficient self-healing, recovering 79% of its mechanical strength after 12 h at room temperature. When applied in a capacitive pressure sensor, the PPG-ERE showed a fast response (220 ms) and recovery (90 ms), detecting forces as low as 3 N. This study provides a practical strategy for designing high-performance multifunctional EREs through soft-segment engineering and dynamic bonding.

Keywords Electrorheological elastomer; Polyurethane; Soft segment; Self-healing; Capacitive pressure sensor

Citation: Yang, Y. B.; Wan, Y.; Zhang, Z. X.; Zhao, Z. J.; Liang, Y. R.; Choi, H. J.; Liu, Y. D. Soft-segment-engineered self-healing polyurethane for high-performance electrorheological elastomers and capacitive sensors. *Chinese J. Polym. Sci.* **2026**, *44*, 2269–2281.

INTRODUCTION

Electrorheological (ER) materials, a class of smart stimuli-responsive systems, have garnered significant interest owing to their ability to rapidly and reversibly tune rheological properties under an applied electric field. Since Winslow's pioneering report of the "electroviscous effect" in 1949, electrorheological fluids (ERFs)—comprising polarizable particles suspended in insulating oils—have been widely investigated,[1] leading to the development of various active particulate materials.[2–5] Nevertheless, liquid-based ERFs suffer from intrinsic limitations, such as particle sedimentation and leakage, which severely restrict their long-term reliability and practical applications.[6–8] To overcome these drawbacks, solid-state analogs known as electrorheological elastomers (EREs) have been developed. The EREs demonstrate enhanced durability and effectively mitigate issues related to particle settling and liquid leakage.[9] Upon electric stimulation, the embedded polarizable particles within the elastomeric matrix attract each other, leading to a swift and notable increase in storage modulus and stiffness.[10] These favorable characteristics make EREs promising for applications in damping, vibration isolation, and actuation technologies.[11,12]

A key metric for evaluating the performance of EREs is ER efficiency, defined as $\left(G'_E - G'_0\right)/G'_0$, where G'_E and G'_0 represent the storage modulus of the ERE with and without an electric field, respectively.[13] Conventional EREs often employ polydimethylsiloxane (PDMS) as the matrix, with silicone oil added as a plasticizer to reduce hardness and thereby enhance the ER efficiency.[14–16] However, such systems often exhibit inadequate mechanical strength, and the plasticizer tends to migrate or leak during operation, which is primarily attributed to the choice of the matrix material.[17] Thermoplastic polyurethane (PU) has recently emerged as an attractive alternative matrix owing to its long service life, low cost, and low environmental impact.[18,19] Nevertheless, most prior studies have focused on reinforcing the mechanical performance of PUs,[20,21] which typically raises the zero-field modulus, which is a disadvantage for the ER efficiency, as the formula favors a lower baseline modulus. Thus, strategically re-

* Corresponding authors, E-mail: zhenjie_shine@163.com (Z.J.Z.)
E-mail: ydliu@ysu.edu.cn (Y.D.L.)
Received January 19, 2026; Accepted March 6, 2026; Published online June 8, 2026

ducing the modulus of PU through chemical design is crucial for advancing high-performance PU-based EREs. However, an excessively low modulus would also undermine practical utility, as many engineering applications require a certain load-bearing capacity. This highlights the delicate balance needed to tune PU's mechanical properties of PU: the modulus must be lowered to boost the ER response while retaining sufficient strength for real-world applications.

To date, efforts to modulate PU mechanics have predominantly focused on hard-segment modifications.[22,23] However, achieving a lower modulus necessitates a greater soft-segment content, underscoring the pivotal yet understudied role of soft-segment chemistry. Polyether polyols, for instance, impart high chain flexibility, yielding PUs with low hardness, good elasticity, and low-temperature resistance.[24] In contrast, polyester polyols offer better biocompatibility and, owing to their semi-crystalline nature, can enhance the mechanical strength in diverse application scenarios.[25] The hydrogen bonding interactions between the soft and hard segments play a critical role in regulating the overall properties of PU.[26] In addition, the soft segments significantly influence the dielectric behavior of PUs, which directly affects the ER response of PU-based ERE.[27] Consequently, a systematic comparison of different soft-segment types is crucial for optimizing the mechanical and ER performance of EREs. Furthermore, by using PU as the matrix of ERE, it becomes relatively straightforward to provide ERE self-healing capabilities[28] thereby tackling the problem of damage repair in real-world applications.

In this study, we designed a series of PUs with different soft segments as the matrix for EREs to elucidate how the soft-segment structure affects the mechanical and ER properties under both on- and off-field conditions. Polyether polyols, poly(propylene glycol) (PPG) and poly(tetramethylene glycol) (PTMG), along with polyester polyol polycaprolactone (PCL), were selected as soft segments, while isophorone diisocyanate (IPDI) constituted the hard segment. To endow the system with self-healing ability, 4,4′-dihydroxydiphenyl disulfide (DHDDS) was incorporated to introduce dynamic disulfide bonds,[29] which together with PU's inherent hydrogen bonds of PU enable reversible network repair.[30,31] Titanium dioxide (TiO_2) particles were then dispersed into the self-healing PU matrix to fabricate the final ERE. This approach is expected to yield EREs that combine a balanced low modulus, enhanced mechanical integrity, reliable self-healing, and a satisfactory ER performance. Moreover, the tailored dielectric properties of these EREs may extend their utility to multifunctional applications such as dielectric layers in capacitive pressure sensors for next-generation wearable electronics.

EXPERIMENTAL

Materials

Poly(propylene glycol) (PPG, M_n=2000), 1,4-butanediol (BDO) and isophorone diisocyanate (IPDI) were purchased from Sigma-Aldrich. Dibutyltin dilaurate (DBTDL) was supplied by Aladdin. Poly(tetramethylene glycol) (PTMG, M_n=2000), 4,4′-dihydroxydiphenyl disulfide (DHDDS) and polycaprolactone (PCL, M_n=2000) were purchased from Macklin. *N*,*N*-dimethylformamide (DMF) was sourced from Tianjin Kermel Chemical Reagent Co., Ltd. Tetrabutyl titanate (TBT) was supplied by TCI Chemicals. Prior to use, PPG, PTMG, PTMG, BDO, and IPDI were dried at 100 °C for 12 h.

Synthesis of Self-healing PU

PPG (10 g) and IPDI (4.11 g) were introduced into a four-necked flask, mechanically stirred at 260 r/min, and heated to 75 °C under a nitrogen atmosphere for 30 min. Subsequently, DBTDL, at 1 wt% of the total reactants was added as a catalyst, and the reaction was allowed to proceed for 2 h to form a prepolymer. that, 1.1 g) was then added to the prepolymer for the first chain-extension step, which proceeded for 2 h. The temperature was then lowered to 45 ℃, and 0.3 g of DHDDS, previously dissolved in DMF, was added for a second chain-extension step, continued for another 2 h. The resulting mixture was poured into a polytetrafluoroethylene (PTFE) mold, degassed several times, and then cured in an oven at 120 °C for 12 h to produce the PU elastomer. The synthesis procedures for the PTMG-based and PCL-based PU were identical to those used for the PPG-based PU.

Fabrication of EREs

First, a certain amount of TiO_2 particles (20 wt% of the total mass) was dispersed in DMF and shaken for 5 min, followed by ultrasonication for 30 min to obtain a well-dispersed suspension. After completing the two-step chain extension of the PU, an appropriate amount of DMF was added to reduce the viscosity of the system. The stirring speed was then increased to 800 r/min, and the TiO_2 suspension was slowly added dropwise, followed by continuous stirring for 2 h. Finally, the homogeneous mixture was cast into a PTFE mold and dried to form the ERE. The synthesis process for the TiO_2 particles is described in Supporting Information.

Characterization

To evaluate the dispersibility of the TiO_2 particles within the PU matrix, the elastomers were fractured at cryogenic temperatures using liquid nitrogen and then coated with a thin layer of gold. The cross-sectional morphology of the EREs was examined using scanning electron microscopy (SEM, S4800-II, Hitachi, Japan). The chemical structures of the elastomers were characterized using Fourier-transform infrared spectroscopy (FTIR, Bruker E55+FRA106, Germany) over a spectral range of 4000–400 cm^{-1} at ambient temperature. The crystalline structures of the PUs and EREs were analyzed using small-angle X-ray scattering (SAXS, Anton Paar SAXS-Point 5.0, Austria) to characterize their nanoscale structural ordering. Thermogravimetric analysis (TGA, Netzsch STA499C-F5, Germany) of the PUs and EREs was carried out under a nitrogen atmosphere at a heating rate of 10 °C/min, ramping from ambient temperature to 700 °C. The glass transition temperatures of the PUs and EREs were determined by differential scanning calorimetry (DSC, DSC 250, USA).

Mechanical Testing

The mechanical properties of the PUs and EREs were evaluated using an electronic universal testing machine (TFW-5S; Tuofeng Instruments, China). The elastomers were cut into dumbbell-shaped specimens with dimensions of 50 mm × 4 mm × 1 mm and subjected to tensile evaluation at a constant displacement rate of 50 mm/min.

https://doi.org/10.1007/s10118-026-3644-3

Self-healing Performance Testing

Samples of the same size as those used for mechanical testing were cut in the middle, and the two fractured ends were brought into contact and placed in a vacuum oven at 25 °C for 12 h. Fracture morphology was examined using an optical microscope (CX43, OLYMPUS, Japan). Self-healed dumbbell-shaped samples prepared in the same manner were subjected to identical mechanical testing. Self-healing efficiency (η) was calculated using Eq. (1):

$$\eta\ (\%) = E_h/E_0 \times 100\% \quad (1)$$

where E_h denotes the tensile strength after self-healing and E_0 denotes the tensile strength without damage.

Rheological Testing

The viscoelastic behavior of the ERE samples was investigated using a rotational rheometer (MCR502, Anton Paar, Austria) equipped with a parallel-plate geometry (PP15/E/Ti/S). The test specimens were prepared in the form of discs with a diameter of 15 mm and thickness of 1 mm. A constant normal force of 1 N was maintained throughout the measurements to ensure the accuracy. Amplitude sweeps were performed at an oscillatory shear frequency of 10 rad/s over a strain amplitude range of 0.01%–10%. Frequency sweeps were performed in the range of 1–100 rad/s at a fixed strain amplitude of 0.01%. During each test, an external electric field was applied in the range of 0–3 kV·mm^{-1} to evaluate the viscoelastic response of the EREs under varying field strengths. The strain-dependent energy dissipation was quantified by the loss factor (tanδ), calculated from the ratio of G'' to G' obtained during the amplitude sweeps. The relative ER efficiency was determined according to Eq. (2):

$$\text{ER efficiency} = \frac{G'_E - G'_0}{G'_0} \times 100\% \quad (2)$$

where G'_E and G'_0 denote the storage moduli of the ERE with and without an applied electric field, respectively.

Dielectric Testing

Before the measurements, the specimens were cut into circular discs with a diameter of 25 mm and a thickness of 1 mm to ensure conformal contact with the electrodes. Dielectric spectroscopy was carried out using an impedance analyzer (SI 1260, Solartron, UK) under an applied AC voltage of 0.1 V, within a frequency range of 0.1–10^6 Hz.

Capacitive Pressure Sensing Performance Testing

Conductive tape was attached to the upper and lower surfaces of the ERE, and wires were connected to an impedance analyzer (IM 3570, Hioki, Japan) to monitor the capacitance variations. The pressure applied under different conditions was quantified using a digital force gauge (ZP-100N; Kehui, China).

For performance evaluation, the assembled capacitive pressure sensor (CPS) was affixed to the back of the hand, and the capacitance variations were recorded during finger tapping and pressing. Furthermore, when the CPS was attached to the thumb, the Morse code signals were successfully transmitted by varying the duration of the finger press. A continuous press was also applied to the surface of the CPS to record the relationship between the capacitance and pressure. The relative capacitance change ($\Delta C/C_0$) was calculated according to Eq. (3):

$$\Delta C/C_0 = \frac{C' - C_0}{C_0} \quad (3)$$

where C' is the varied capacitance and C_0 is the initial capacitance.

RESULTS AND DISCUSSION

Structures of Synthesized EREs

Fig. 1(a) illustrates the preparation process of EREs. To elucidate the role of soft-segment structures in PU, three polyols with distinct architectures were incorporated. Polyether-based segments (PPG and PTMG) imparted high chain mobility, whereas the polyester segment (PCL) contributed to enhanced mechanical strength owing to its semi-crystalline nature. Moreover, the alicyclic structure of IPDI introduces appropriate steric hindrance, further promoting chain mobility. This structural design facilitated dynamic disulfide exchange in DHDDS, thereby endowing the PU matrix with self-healing capabilities (Fig. 1b). In addition, the dielectric nature of the PU matrix with embedded TiO_2 particles enhanced the capacitive sensing performance of the elastomer (Fig. 1c).

FTIR spectroscopy was employed to verify the chemical reactions and molecular interactions within PUs- and PU-based EREs. As shown in Figs. 2(a) and 2(b), the disappearance of the characteristic isocyanate (—NCO) absorption band at 2270 cm^{-1} confirmed the complete consumption of isocyanate groups during the polymerization process. Carbonyl (—C=O) stretching vibrations were observed in the range of 1760–1660 cm^{-1}, while a broad absorption band corresponding to —NH stretching appeared near 3300 cm^{-1}. In addition, the presence of a distinct disulfide (—S—S—) stretching band at 760 cm^{-1} verified the successful incorporation of disulfide linkages.[21] Notably, the carbonyl stretching bands observed between 1760 and 1660 cm^{-1} were associated with hydrogen bonding interactions among the hard segments. As shown in Fig. 2(c), the incorporation of TiO_2 particles resulted in a pronounced reduction in the intensity of these bands, suggesting that the particles interfered with the hydrogen bond formation within the hard domains. The adsorption peaks in the range of 1760–1650 cm^{-1} were fitted by the Gauss-Lorentz curve, as shown in Fig. 2(d). The peak in the range of 1710–1725 cm^{-1} (peak 1) corresponds to the free carbonyl stretching vibrations, while the peak observed near 1695 cm^{-1} (peak 2) is associated with strongly hydrogen-bonded carbonyl groups.[32] The characteristics and intensities of these hydrogen-bonded carbonyl peaks vary significantly depending on the type of the soft segment. At the same observation scale, the carbonyl vibration intensity in PPG-PU was the weakest, indicative of the lowest hydrogen bonding strength, which was attributed to the steric hindrance of its methyl (—CH_3) side groups. Conversely, PCL exhibited the highest carbonyl vibration intensity, likely because of the presence of a large number of ester groups, as urethane-ester hydrogen bonds possess greater bond energies than urethane-ether bonds. Because PTMG lacks side groups that cause steric interference, the hydrogen bonding strength in PTMG-based systems is greater than that in PPG-based systems, contributing to enhanced mechanical properties. To quantitatively assess the extent of hydrogen bonding

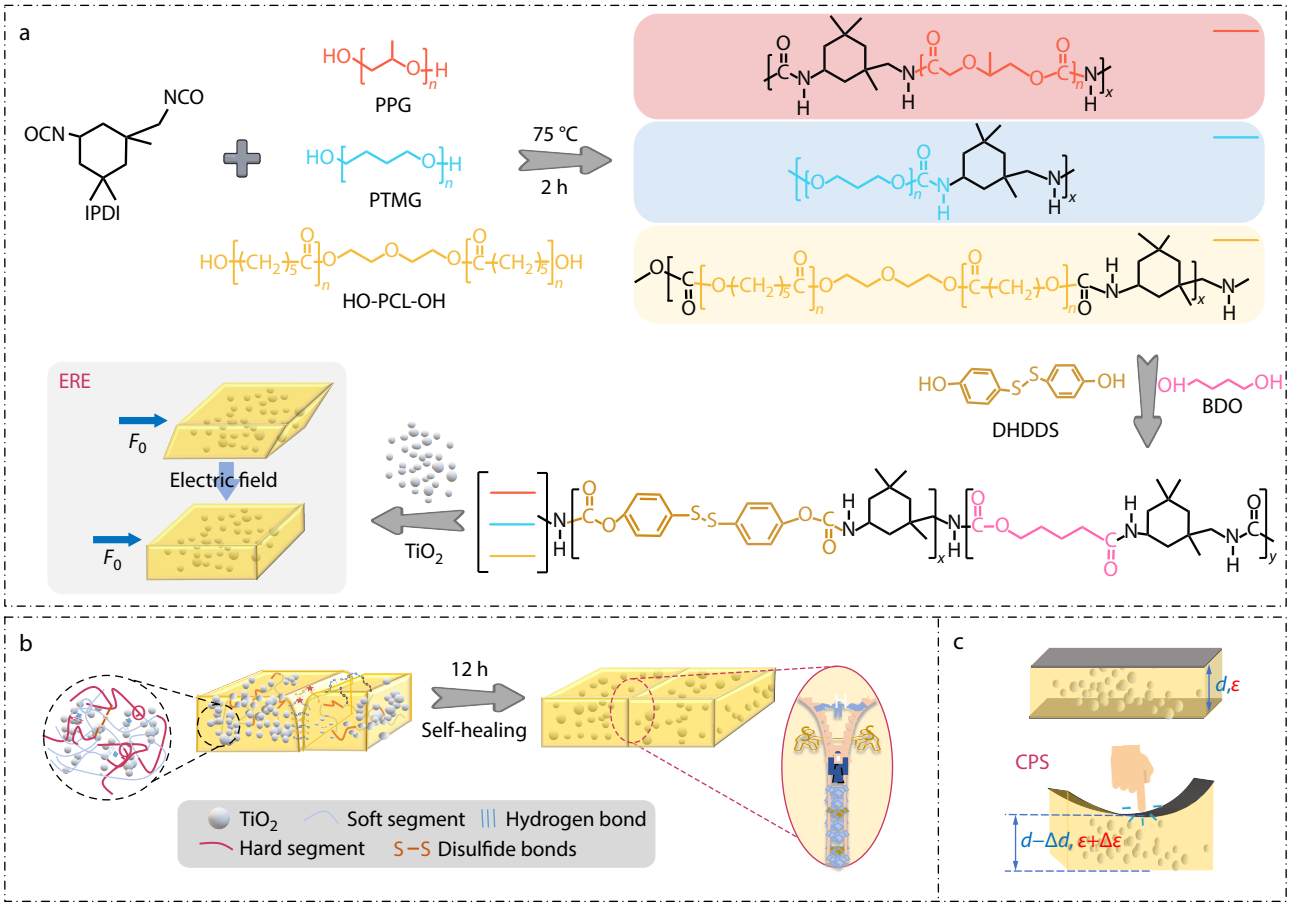

Fig. 1 Construction and characterization of the EREs. (a) Preparation of EREs; (b) Schematic illustration of the self-healing mechanism of EREs; (c) Schematic representation of the working mechanism of CPS with a composite elastomer active layer.

associated with the urethane carbonyl groups present in PUs and PU-based EREs, the hydrogen bonding content (X) was calculated using the peak areas[33,34]

$$X = \frac{A_h}{A_h + A_f} \times 100\% \quad (4)$$

where A_h and A_f are the peak areas of the H-bonded and free carbonyl groups, respectively. Table S1 (in the electronica supplementary information, ESI) presents the X values for all the PU and ERE samples. It is important to emphasize that X represents the relative ratio of the hydrogen-bonded carbonyl groups rather than an absolute measurement. PTMG-PU demonstrated the highest hydrogen bonding content of 79.75%, which was attributed to the high regularity of the PTMG soft segment. In contrast, PPG-PU exhibited the lowest hydrogen bonding content (6.27%), likely because of the significant steric hindrance imposed by the methyl side groups. Among the ERE samples, PTMG-ERE also displayed the highest X value (69.43%).

Thermogravimetric (TG) and derivative thermogravimetric (DTG) analyses were performed to further validate the thermal stability of the prepared samples. As illustrated in Figs. 3(a) and 3(b), the chemical structure of the soft segments had a significant impact on the thermal properties of both PUs. Polyether polyols (PPG and PTMG) offer better flexibility, which facilitates greater chain mobility and results in lower thermal degradation rates and higher thermal stabilities.[35] Notably, the thermal decomposition temperature of the soft segments was significantly higher than that of the hard segments. Therefore, the samples containing PPG and PTMG as soft segments, which demonstrated lower compatibility with the hard segments, exhibited two distinct decomposition peaks. These samples also indicated a greater residual mass at equivalent temperatures relative to PCL-PU, indicating higher thermal stability. In the case of PCL-PU, a single decomposition peak near 340 °C was observed, which was attributed to the favorable compatibility between PCL and the hard segments. After TiO_2 incorporation (Figs. 3d and 3e), the decomposition peaks associated with various soft segments shifted toward lower temperatures, accompanied by a reduction in the temperature differential between the decomposition of the soft and hard segments. This indicates that the TiO_2 particles disrupted intermolecular interactions, thereby enhancing segmental compatibility and diminishing the degree of microphase separation.

Figs. 3(c) and 3(f) show the determination of the glass transition temperature (T_g) of the PUs and PU-based EREs using DSC thermograms. In the PU elastomer containing PCL as the soft segment, a melting peak corresponding to crystallization was observed at 34.11 °C, indicating the presence of crystalline domains. The addition of the TiO_2 particles disrupted these crystalline regions, leading to the disappearance of the melting peak. The T_g of PU containing PPG and PTMG, associ-

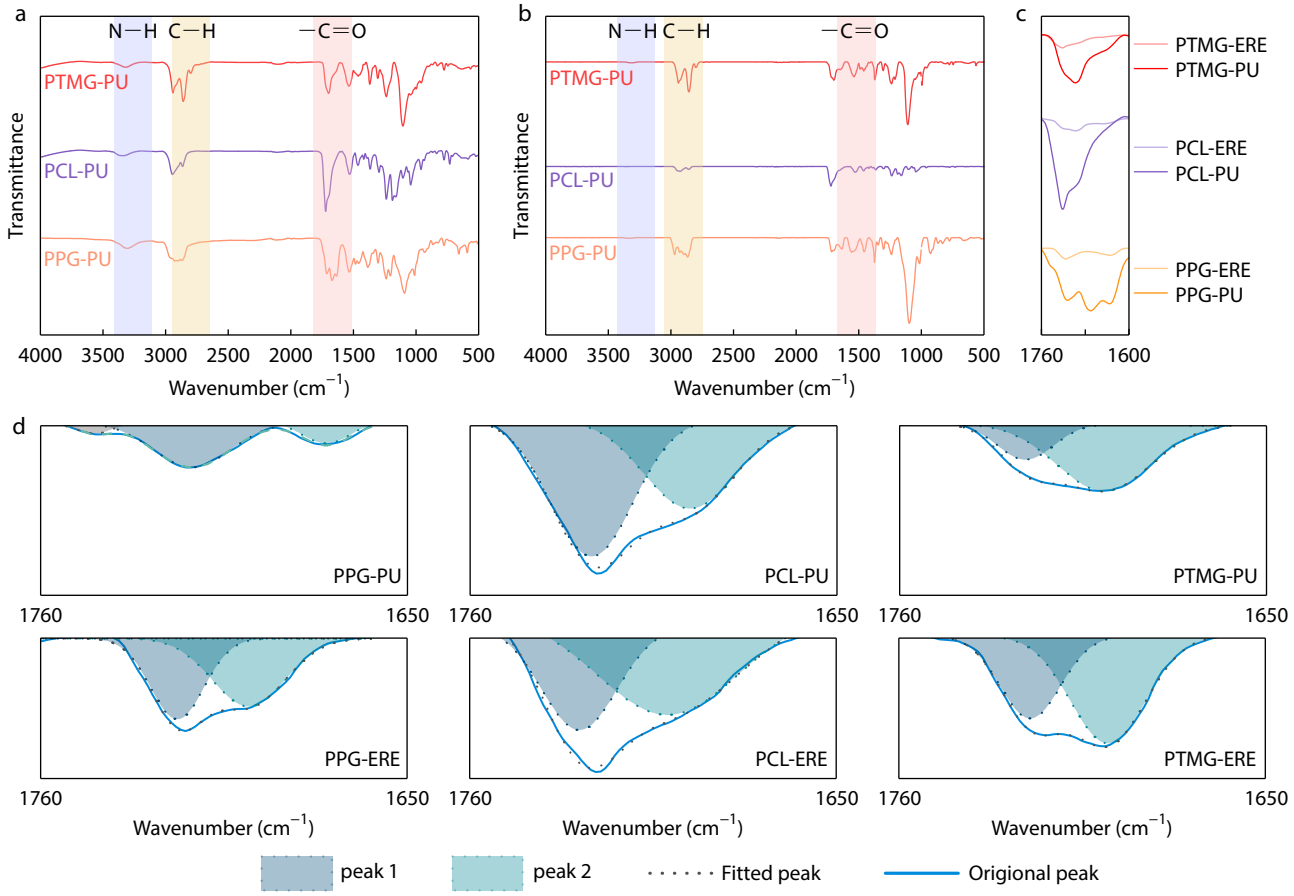

Fig. 2 FTIR spectra of the (a) PUs, (b) 20 wt% TiO_2-filled EREs, and (c) the comparison spectra in the range of 1760–1660 cm^{-1} for the PUs and EREs; (d) Peak separation simulation in the range of 1760–1660 cm^{-1} for the PUs and EREs.

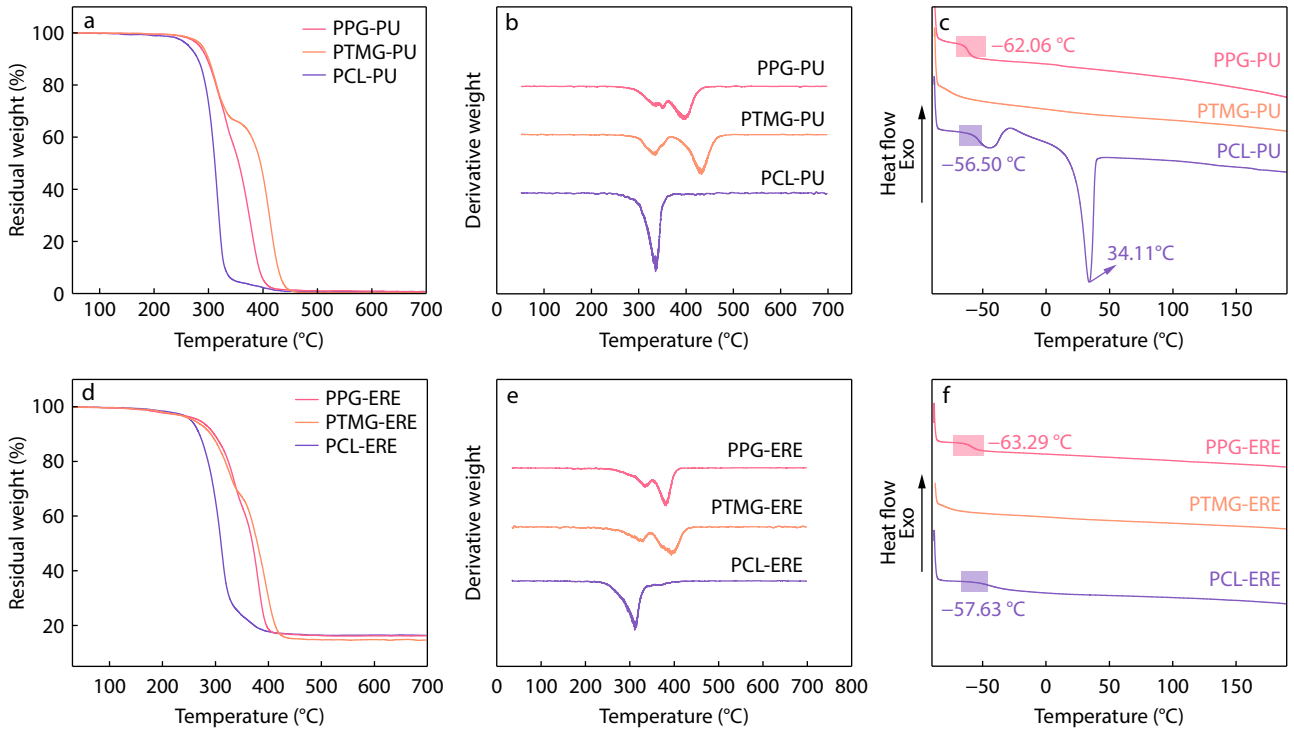

Fig. 3 Thermal analysis of PUs and EREs: (a) TG, (b) DTG and (c) DSC curves of PUs; (d) TG, (e) DTG and (f) DSC curves of EREs.

https://doi.org/10.1007/s10118-026-3644-3

ated with chain mobility within the soft segments, exhibited a downward shift following the incorporation of TiO_2 particles. This reduction was ascribed to the disruption of intermolecular interactions caused by the particles, thereby enhancing the segmental mobility of the PU soft segments to some extent. The SAXS analysis (Fig. S1 in ESI) revealed a weak scattering peak in the q range of 0.50–0.75 nm^{-1} for the PUs, indicating the presence of limited microphase separation. Upon incorporation of TiO_2 particles, the scattering peak was significantly suppressed, suggesting that the particles interfered with intermolecular interactions among chain segments and consequently diminished the degree of microphase separation.

Fig. 4 shows the cross-sectional SEM images of the EREs, indicating the dispersion of TiO_2 particles within the PU matrix. As it has been observed that the synthesized TiO_2 particles exhibit a tendency to aggregate, with the majority displaying diameters ranging from 0.5 μm to 2.0 μm (Fig. S2 in ESI). As shown in Figs. 4(a)–4(c), the SEM images of the ERE cross-sections demonstrate a similar distribution of TiO_2 particles across the EREs based on different soft segments, with the absence of large agglomerates. This observation suggests that the interaction between the TiO_2 particles and PU matrix not only affects the interactions among the polymer chains but also inhibits the formation of particle agglomerates.

Mechanical Properties of PUs and EREs

Figs. 5(a) and 5(b) show the tensile properties of PUs and EREs with varying soft-segment structures. Among the three PU elastomers, PCL-PU exhibited the highest tensile strength (12.33 MPa, whereas its corresponding ERE exhibited the highest tensile strength (9.45 MPa among the three EREs samples. This superior mechanical performance can be attributed to the pronounced crystallization tendency of PCL. The FTIR analysis further revealed stronger hydrogen bonding in PCL-PU, which contributed to its superior mechanical strength. However, the presence of crystalline domains markedly restricts polymer chain mobility, limiting chain extension and deformation and resulting in reduced elongation at break. In contrast, samples based on PPG displayed the largest elongation at break, reaching up to 1835% for PPG-ERE. The methyl ($-CH_3$) side groups resulted in a relatively weak hydrogen bonding strength in the PPG-based samples and finally led to the lowest tensile strength of 3.6 MPa for PPG-ERE. PTMG, which is characterized by its $-C-O-C-$ structure and the absence of side groups interfering with hydrogen bonding, exhibits intermediate mechanical properties. Compared to the EREs with the other two soft segment structures (PPG-ERE and PCL-ERE), PTMG-ERE has a higher mechanical strength (6.5 MPa and greater elongation at break (1125%). Fig. 5(c) illustrates the significant differences in Young's modulus among the PU elastomers, consistent with the influence of the chain segment structure and hydrogen bond strength discussed previously. PPG-PU exhibits the lowest modulus at 4.83 MPa, followed by PTMG-PU at 10.33 MPa, with PCL-PU displaying the highest modulus of 15.30 MPa. In the ERE samples, the incorporation of TiO_2 particles leads to a reduction in Young's modulus, which is attributed to a marked decrease in hydrogen bond strength and the introduction of additional free volume by the particles.

Figs. 5(d) and 5(e) provide a more intuitive demonstration of the macroscopic mechanical performance. A thin-film specimen with dimensions of 25 mm × 4 mm × 0.5 mm and a mass of about 0.5 g was able to support a load of 700 g—approximately 1400 times its own weight—without fracturing, thereby highlighting its remarkable load-bearing capacity. In addition, the sample readily withstood punctures by sharp objects without exhibiting cracks or structural failure. These findings confirm that engineered PU-based EREs possess outstanding overall mechanical stability and damage resistance,

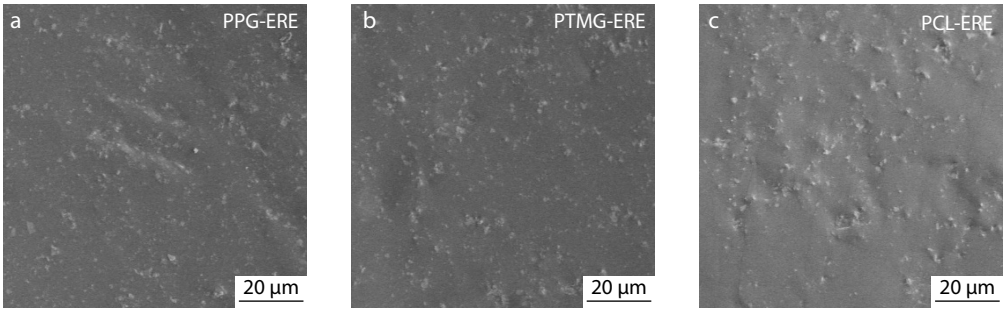

Fig. 4 Cross-sectional SEM images of EREs: (a) PPG-ERE, (b) PTMG-ERE, and (c) PCL-ERE.

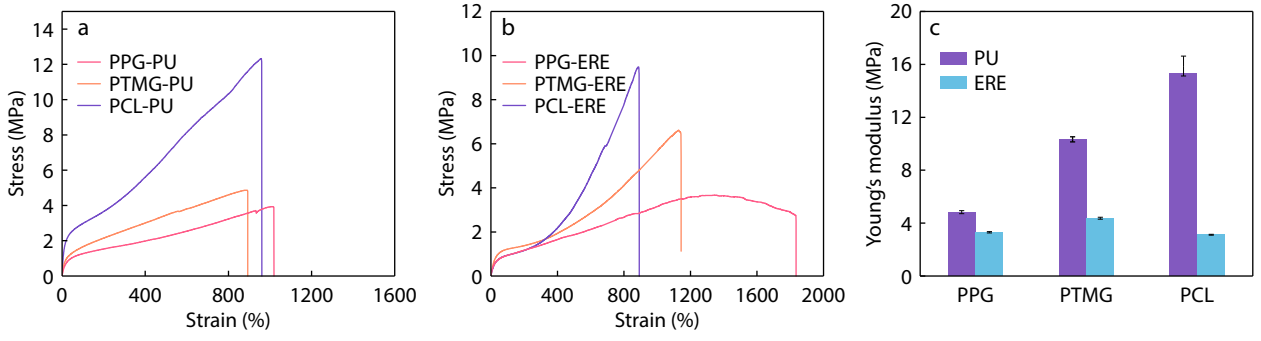

https://doi.org/10.1007/s10118-026-3644-3

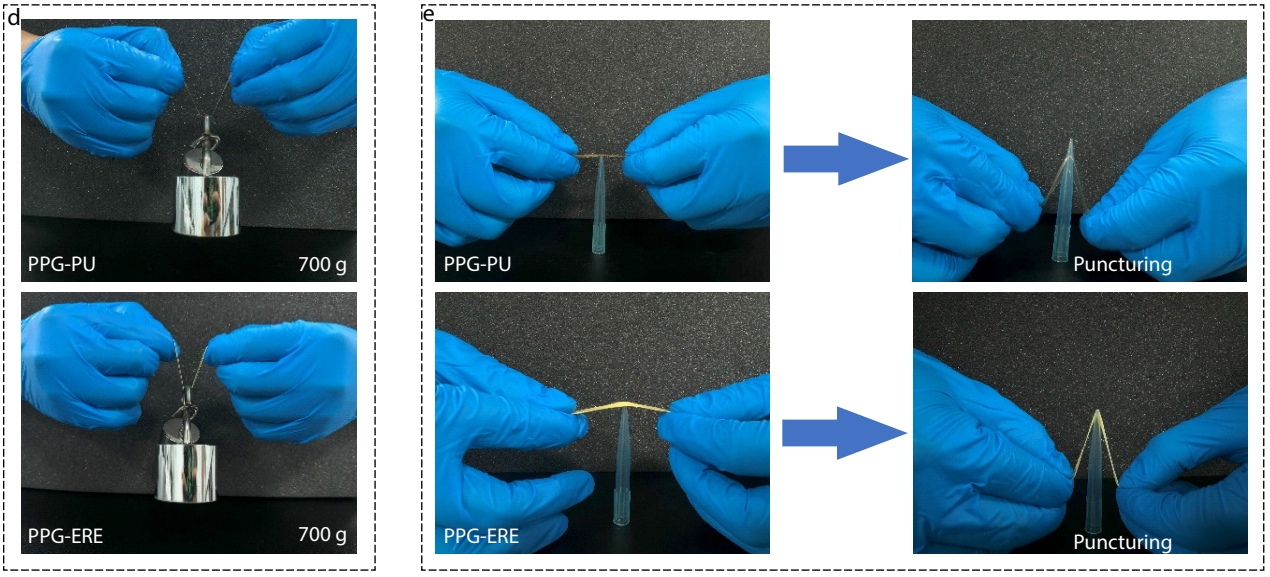

Fig. 5 Mechanical properties of PUs and EREs. (a, b) Stress-strain curves of PUs and EREs; (c) Young's modulus of PUs and EREs; (d) Load-bearing test showing support of 1400 times its own weight for PPG-PU and PPG-ERE; (e) Puncture resistance performance of PPG-PU and PPG-ERE.

providing compelling evidence of their reliability for practical applications.

Self-healing Performance of PUs and EREs

The self-healing properties of polymeric materials are fundamentally governed by two key factors: (i) the existence of dynamic and reversible physical/chemical bonds, and (ii) elevated chain mobility. In PUs, hydrogen-bonding interactions between soft and hard segments, together with disulfide bonds, establish essential conditions for effective healing. The alicyclic diisocyanate IPDI provided an optimal balance by introducing moderate steric hindrance that facilitated chain rearrangement while simultaneously enhancing the mechanical robustness of the material. In EREs, the incorporation of particles further modulates both dynamic bond interactions and chain mobility, underscoring the critical role of selecting a suitable soft segment to optimize the healing efficiency. The optical microscopy images in Fig. S3 (in ESI) demonstrate that PUs are capable of closing surface cracks within 12 h at room temperature without the application of any external stimuli. Among the samples, PPG-ERE exhibited the highest self-healing efficiency, recovering a tensile strength of 2.8 MPa and elongation at break of 1000%, as shown in Fig. 6(a), achieving a self-healing efficiency of 79%. This superior performance is attributed to the presence of

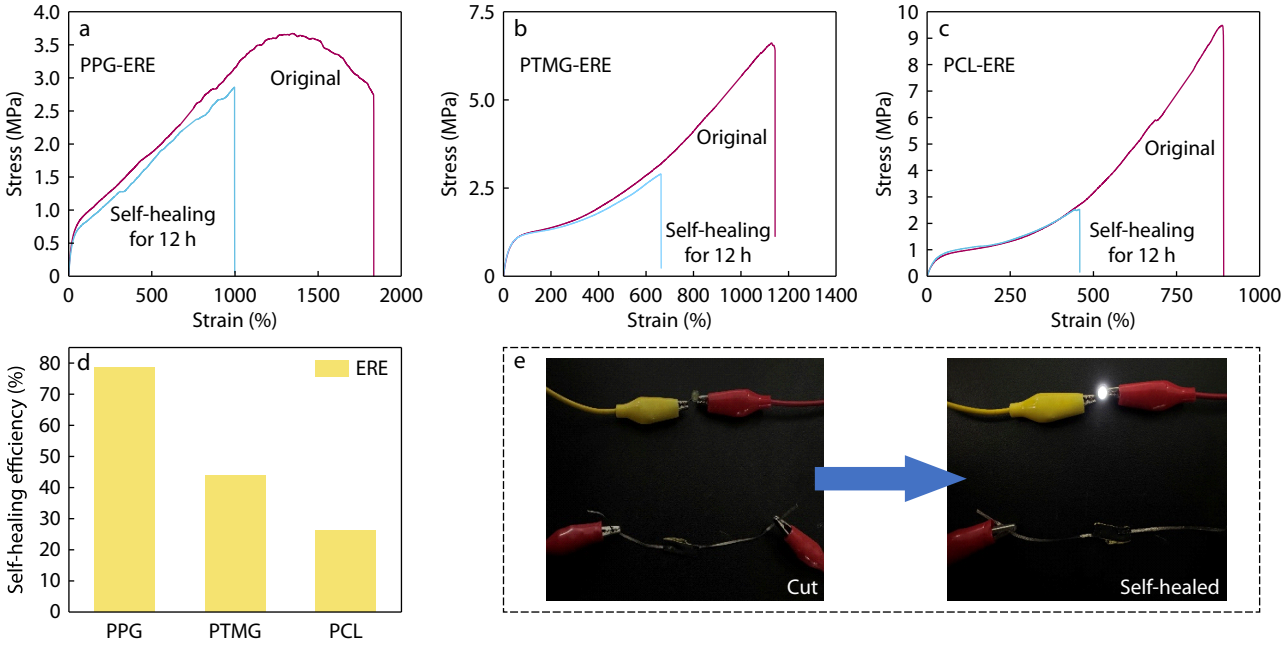

Fig. 6 Self-healing performance of EREs. (a–c) stress-strain curves of the original and self-healed (12 h) ERE samples; (d) Self-healing efficiency of EREs; (e) Rapid self-healing and functional recovery of PPG-ERE in the circuit.

https://doi.org/10.1007/s10118-026-3644-3

—CH_3 groups in PPG, which enhance chain flexibility and enable more effective conformational adjustments. Relatively weak hydrogen bonding facilitates the reversible breaking and reformation of physical bonds. For PTMG-ERE, despite the high original tensile strength, particle incorporation impeded the achievement of higher tensile strength upon healing; the self-healed PTMG-ERE exhibited a tensile strength of 2.85 MPa and elongation at break of 665% (Fig. 6b). PCL-ERE showed the lowest healing efficiency, attributable to restricted chain dynamics (Fig. 6c). The overall self-healing efficiencies are summarized in Fig. 6(d), confirming that PPG-ERE had the highest efficiency, whereas PCL-ERE had the lowest efficiency. Furthermore, Fig. S4 (in ESI) shows the stress-strain curves of PPG-PU after self-healing compared to the original sample. A significantly higher self-healing efficiency of 91.8% was achieved, indicating that the mobility and interaction of the polymer chains were reduced by the incorporation of TiO_2 particles.

The self-healing functionality of the EREs was further validated through a bulb lighting experiment, as depicted in Fig. 6(e). When the conductive carbon black layer was intact, the bulb was illuminated, confirming the presence of a closed electrical circuit. The disruption of this layer interrupted the conductive pathway, leading to the extinction of the bulb. Remarkably, after self-healing at 70 °C for only 1 min, the film fully restored its electrical conductivity, enabling the bulb to relight. This rapid recovery demonstrates the capability of EREs to restore electrical functionality under mild conditions, thereby underscoring their potential as intelligent self-healing materials for flexible electronics.

Viscoelastic Properties of EREs

Fig. 7 shows the strain sweep profiles of the storage modulus (G') and loss modulus (G'') for the EREs subjected to varying electric field strengths, and the frequency sweep results are shown in Fig. S5 (in ESI). Within the strain range of 0.01%–10%, G' consistently exceeded G'', demonstrating the dominant elastic behavior of the material.[36] For EREs with polyether polyols as soft segments, namely PPG-ERE (Fig. 7a) and PTMG-ERE (Fig. 7b), both G' and G'' remained nearly constant within 0.01%–1% strain, followed by a slight decline beyond 1%, while still remaining within the linear viscoelastic region. This behavior suggests that the polymer chain networks retain recoverability under shear deformation, which is attributed to the higher flexibility of polyether polyols, which enables the rapid reconstruction of deformed chains. At elevated strains, the delayed chain mobility impedes structural recovery, resulting in reduced moduli. In contrast, the PCL-ERE samples exhibited a pronounced decrease in the modulus near 2.12% strain and a smaller difference between G' and G'' (Fig. 7c). This behavior is ascribed to the strong crystallization tendency of PCL; the crystalline domains hinder their structural reformation, leading to reduced rigidity and lower modulus.

The loss factor, which is closely related to the viscoelasticity of polymers,[37] was evaluated to analyze the rheological characteristics of the EREs under varying strains. As shown in Figs. 7(d)–7(f), increasing the strain enhanced the molecular chain motion and interfacial slippage between the polymer chains and TiO_2 particles, leading to increased energy dissipation and thus an increase in the loss factor. However, the PPG-ERE exhibited the lowest loss factor with minimal variation with increasing strain. This can be attributed to the relatively weak hydrogen bonding in PPG-ERE, which reduces the friction generated during interfacial slippage between the molecular chains and particles, leading to lower energy dissipation.

Fig. 8(a) shows that the G' of the EREs increases with the ap-

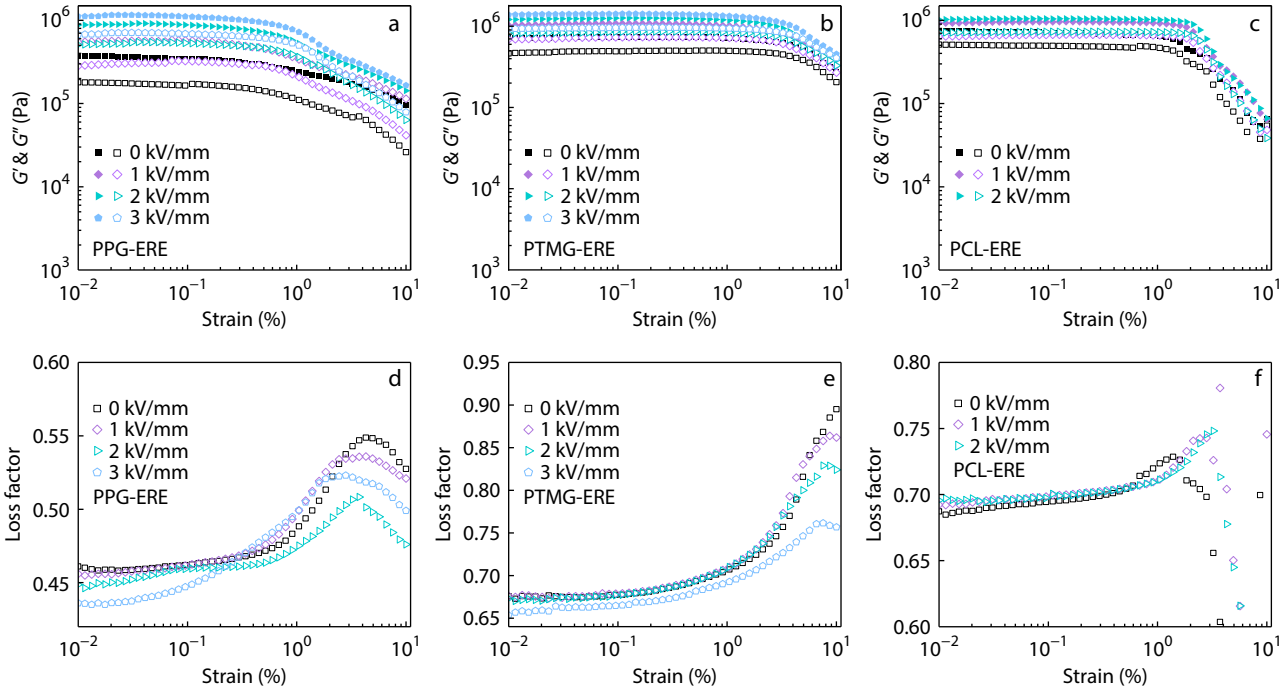

Fig. 7 Rheological properties of EREs. (a–c) The dependance of storage modulus (G') (solid symbols) and loss modulus (G'') (open symbols) on strain amplitude under different electric field strength; (d–f) The loss factor (tanδ) in strain amplitude sweeps.

plied electric field strength. This enhancement is ascribed to the field-dependent polarization of the TiO_2 particles and their interactions with the surrounding particles, resulting in increased hardness and modulus of the EREs. The relative ER efficiency, which is a key metric for evaluating the ER performance, is shown in Fig. 8(b). PPG-ERE achieves the highest ER efficiency of 229.4% at an electric field of 3 kV/mm, with its modulus increasing from 0.34 MPa to 1.12 MPa. This is because the PPG-ERE has a lower zero-field modulus, and the high elasticity and mobility of its flexible soft segments facilitate greater contraction under an electric field. PTMG-ERE displays an ER efficiency of 74.3%, even though, the highest G' of 1.43 MPa at 3 kV/mm is achieved in this sample. In contrast, the PCL-ERE is prone to dielectric breakdown at 3 kV/mm and attains an ER efficiency of only 48% at 2 kV/mm, which is consistent with the highest dielectric constant and dielectric loss discussed below. These results indicate that the polyether-type soft-segment composition enhances ER performance. EREs with more flexible soft segments exhibited a wider linear viscoelastic region, accommodating larger strain variations. Through the engineering of soft segments, the achieved ER efficiency and high field-induced storage modulus were significantly higher than those reported for dipole-dominated and anisotropic EREs.[36]

Dielectric Properties of PUs and EREs

The dielectric properties critically influence the ER performance of EREs. As shown in Fig. 9(a), PPG-PU exhibited a higher dielec-

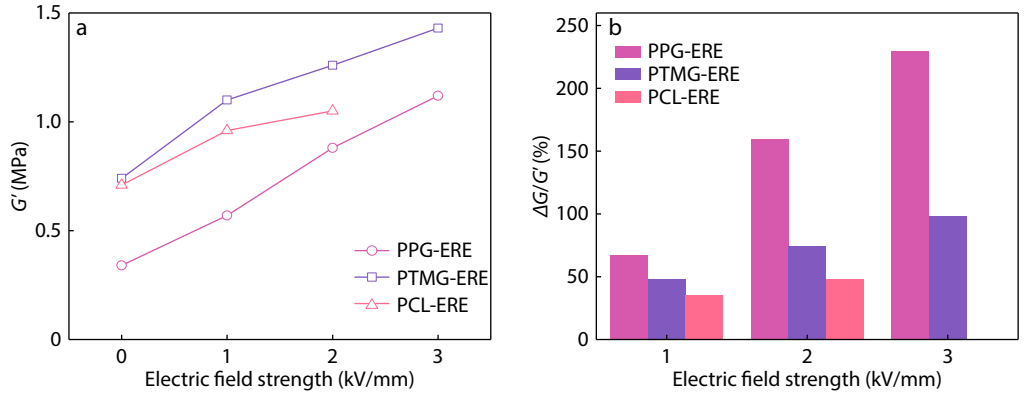

Fig. 8 (a) G' as a function of electric field strength of the EREs; (b) The relative ER efficiency as a function of electric field strength for EREs.

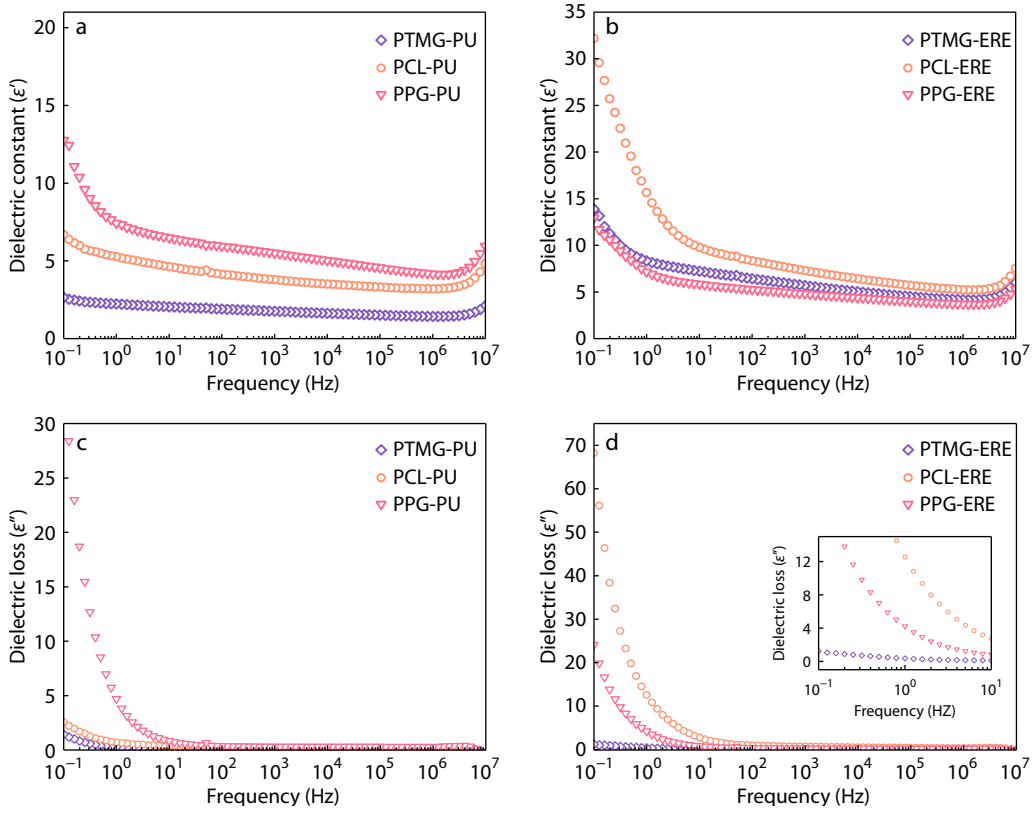

Fig. 9 Dielectric properties of PU and EREs: (a, b) dielectric constant and (c, d) dielectric loss factor.

https://doi.org/10.1007/s10118-026-3644-3

tric constant (5.94 at 100 Hz than PCL-PU (4.14, 100 Hz) and PTMG-PU (1.89 at 100 Hz). This is attributed to the side methyl group of PPG, which improves the mobility of the chain segments, thus increasing the orientational polarization of the polar urethane groups under an electric field. Even though PCL has polar C=O groups, its crystallization tendency results in a non-polar crystalline structure with oppositely oriented dipoles, counteracting polarization, and limiting dipolar contribution at low frequencies, thereby reducing the dielectric constant.[38,39] The non-polar characteristics of PTMG, combined with its enhanced structural regularity, contribute to an increased packing density of the polymer chains, resulting in reduced polarizability. Fig. 9(b) shows that the dielectric constant of the EREs increases after the addition of TiO_2, as TiO_2 is a high-permittivity material that enhances interfacial polarization. In PCL-ERE, the particle fillers disrupt the crystallinity, increasing the dipolar polarization contribution and significantly increasing the dielectric constant. Fig. 9(c) indicates that PPG-PU has a higher dielectric loss, which may be attributed to its lower polarity and higher flexibility. These characteristics result in a stronger molecular mobility, more pronounced polarization lag, and increased internal dissipation under the influence of an electric field.[40,41] After TiO_2 incorporation (Fig. 9d), the dielectric loss of the EREs increases, possibly due to interfacial polarization relaxation and particle aggregation. The higher dielectric loss observed in the PCL-ERE is because the polar ester linkages restrict the chain mobility, preventing efficient polarization reversal under an AC field. In contrast, the lower loss of the polyether analog arises from its flexible chains, which enable rapid dipole reorientation and reduced energy dissipation.

Capacitive Pressure Sensing Performance of EREs

A CPS was fabricated using the PPG-ERE as the dielectric layer (Fig. 10a). The applied pressure induces changes in the capacitance according to the relationship $C = \varepsilon A/d$, where ε is the permittivity of the dielectric sandwich layer situated between the parallel plate electrodes, A denotes the overlapping area of the capacitor plates, and d corresponds to the distance between the electrodes. This configuration enables pressure-sensing functionality. Relative capacitance change ($\Delta C/C_0$) under different pressures was characterize.[42,43] As illustrated in Fig. 10(b), the

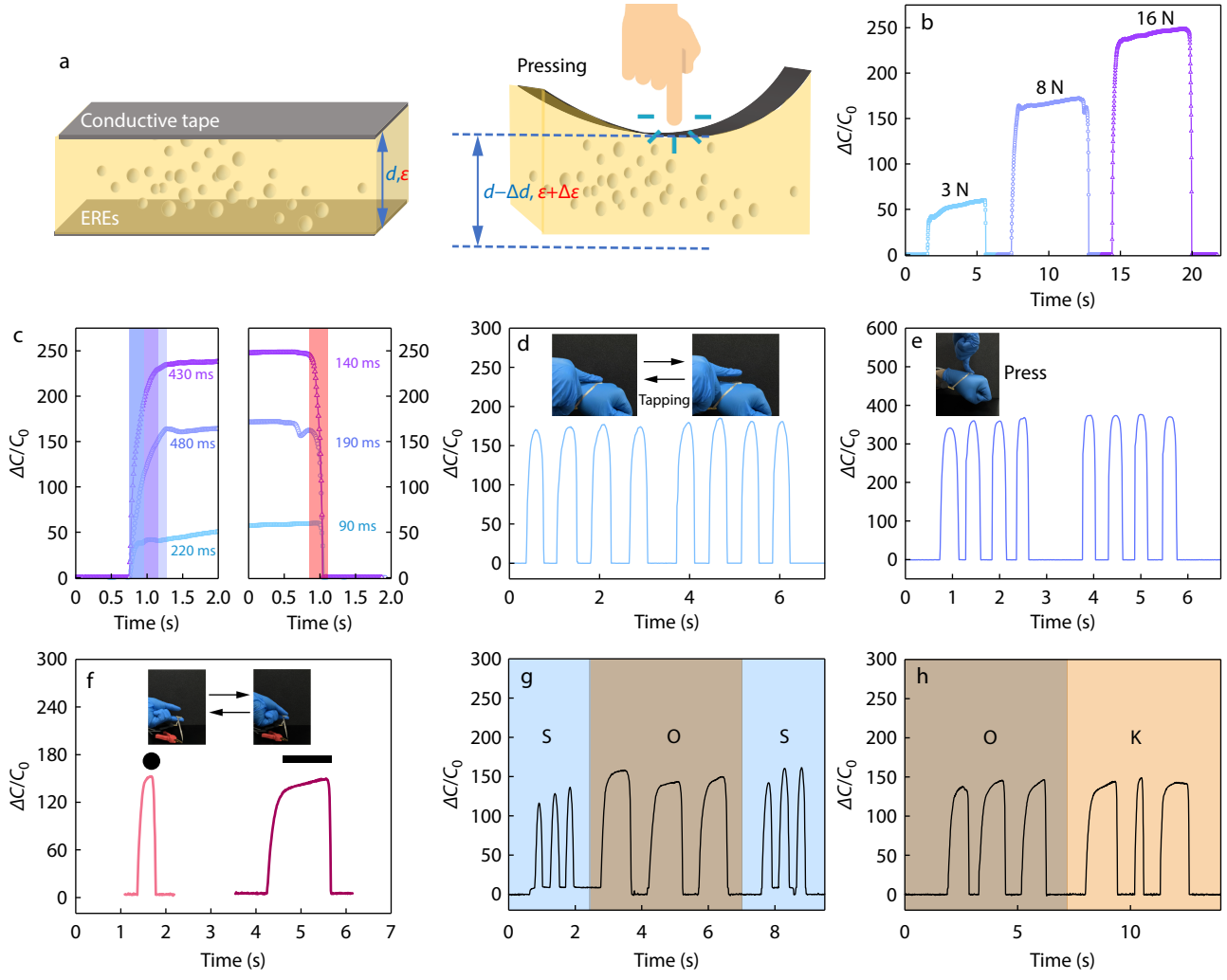

Fig. 10 The performance of PPG-ERR in a capacitive pressure sensor. (a) Schematic representation of the working mechanism of CPS with composite elastomer active layer; (b, c) The capacitance changes of CPS under a force of 3 N; (d, e) Capacitance changes of the CPS under different contact modes; (f–h) Output of "SOS" and "OK" signals by Morse code.

https://doi.org/10.1007/s10118-026-3644-3

CPS exhibits continuous and stable responses over approximately 5 s when subjected to applied forces of 3, 8, and 16 N. The relationship between $\Delta C/C_0$ and applied pressure over a broad pressure range is shown in Fig. S6 (in ESI). This demonstrates a notably high sensitivity during the initial compression state. However, when the pressure increased to 20 N, the capacitance stabilized and did not vary with pressure, which can be attributed to the limited compressive capacity of the elastomer. Fig. 10(c) reveals that both the response and recovery times increase with pressure, ranging from 220 ms to 430 ms for the response time and from 90 ms to 140 ms for the recovery time, consistent with the loss factor analysis. At lower pressures, the sensor exhibited predominantly elastic behavior, resulting in a rapid response. In contrast, higher pressures induced greater vertical strain within the EREs, leading to increased capacitance variation but slowed recovery owing to enhanced viscous dissipation and structural disruption, as depicted in Figs. 10(d) and 10(e). In addition, the CPS enables the transmission of Morse code signals by modulating the duration of the applied force (Figs. 10f–10h). In summary, CPSs fabricated from EREs exhibit rapid response, reliable recovery, and stable signal output across a range of loading conditions. These features highlight the strong potential for integration into wearable electronics and intelligent sensing systems.

CONCLUSIONS

In this study, self-healing PU matrices with different soft-segment structures were synthesized and further integrated with TiO_2 to develop high-performance EREs. The resulting EREs exhibited superior mechanical properties while simultaneously delivering excellent ER responsiveness, self-healing capability, and pressure-sensing functionality. Notably, the ERE incorporating flexible PPG as the soft segment achieved a maximum ER efficiency of 229.4% under an electric field of 3 kV/mm, while maintaining a tensile strength of 3.6 MPa together with an exceptionally high elongation at break of 1835% and a self-healing efficiency of 79%. In contrast, the ERE based on PTMG exhibited a lower ER efficiency of 74.3% but attained the highest storage modulus at 3 kV/mm, likely attributable to an elevated off-field shear modulus arising from the hydrogen-bonded polymer chains. The ERE-containing PCL displayed the greatest tensile strength (9.45 MPa and a higher off-field shear modulus, which corresponded with the lowest ER efficiency, primarily because of the crystallinity inherent in the PCL segments. These outstanding mechanical and self-healing properties expand the practical applicability of EREs and substantially prolong their service life. In addition, EREs have been employed as dielectric layers in the development of CPS. By leveraging the dielectric elastomer characteristics of the EREs, a CPS was fabricated, which exhibited a rapid response to a 3 N external force within 220 ms and recovery within 90 ms, while maintaining a stable signal output under continuous loading. This study demonstrates the feasibility of soft-segment engineering in PU-based EREs and offers new insights into the design of high-performance multifunctional EREs.

Conflict of Interests

The authors declare no interest conflict.

Electronic Supplementary Information

Electronic supplementary information (ESI) is available free of charge in the online version of this article at http://doi.org/10.1007/s10118-026-3644-3.

Data Availability Statement

The related data of this study can be obtained from the corresponding authors for reasonable reasons.

ACKNOWLEDGMENTS

This work was financially supported by the National Natural Science Foundation of China (No. 52372293) and the S&T Program of Hebei Province (No. 244A1001D).

REFERENCES

1 Hao, T. Electrorheological fluids. *Adv. Mater.* **2001**, *13*, 1847–1857.
2 Wen, W. J.; Huang, X. X.; Yang, S. H.; Lu, K. Q.; Sheng, P. The giant electrorheological effect in suspensions of nanoparticles. *Nat. Mater.* **2003**, *2*, 727–730.
3 Choi, H. J.; Jhon, M. S. Electrorheology of polymers and nanocomposites. *Soft Matter* **2009**, *5*, 1562–1567.
4 Ma, R.; Nie, W.; Wang, Y.; Hu, X.; Zhao, X.; Yin, J. Mixed ionic–electronic covalent organic frameworks as a platform for high-performance electro-responsive smart materials. *Chem. Mater.* **2024**, *36*, 6961–6972.
5 Chen, S.; Kuznetsov, N. M.; Hou, L. T.; Choi, H. J.; Zhang, K.; Zhao, J. P.; Li, Y. Limited electron-dominated electrorheological response with TiO2 buffer layer. *Nano Lett.* **2025**, *25*, 5591–5598.
6 Kuznetsov, N. M.; Kovaleva, V. V.; Belousov, S. I.; Chvalun, S. N. Electrorheological fluids: from historical retrospective to recent trends. *Mater. Today Chem.* **2022**, *26*, 101066.
7 Munteanu, L.; Munteanu, A.; Sedlacik, M. Electrorheological fluids: a living review. *Prog. Mater. Sci.* **2025**, *151*, 101421.
8 Chen, S.; Shi, Y. X.; Zhang, K.; Choi, H. J.; Zhao, J. P.; Li, Y. Advancements in electrorheological fluid: from structural engineering to practical application. *Adv. Colloid Interface Sci.* **2026**, *348*, 103736.
9 Liang, Y.; Huang, D.; Zhou, X.; Wang, Z.; Shi, Q.; Hong, Y.; Pu, H.; Zhang, M.; Wu, J.; Wen, W. Efficient electrorheological technology for materials, energy, and mechanical engineering: from mechanisms to applications. *Engineering* **2023**, *24*, 151–171.
10 Ma, N.; Yao, Y. W.; Wang, Q.; Niu, C. G.; Dong, X. F. Properties and mechanical model of a stiffness tunable viscoelastic damper based on electrorheological elastomers. *Smart Mater. Struct.* **2020**, *29*, 045041.
11 Li, H.; Gao, T. Y.; Wang, M.; Zhang, W. L. Approach on the vibration damping and energy absorption through electrorheological/magnetorheological effects. *Sustain. Mater. Technol.* **2025**, *44*, e01401.
12 Xu, Y. J.; Wen, J.; Burdet, E.; Taghavi, M. Monolithic electrostatic actuators with independent stiffness modulation. *Nat. Commun.* **2025**, *16*, 1174.
13 Ti, G.; Fan, Y.; Tang, J.; Niu, C.; Xiong, X. Preparation and enhanced electrorheological properties of elastomers filled with rod-shaped TiO2 particles. *Front. Mater.* **2023**, *10*, 1331513.
14 Liu, B.; Shaw, M. T. Electrorheology of filled silicone elastomers. *J.*

Graphical Abstract

Soft-segment-engineered Self-healing Polyurethane for High-performance Electrorheological Elastomers and Capacitive Sensors

Yan-Bo Yang, Yao Wan, Zi-Xuan Zhang, Zhen-Jie Zhao, Yong-Ri Liang, Hyoung Jin Choi, and Ying-Dan Liu

Yanshan University, China; Inha University, Korea

High-performance self-healing electrorheological elastomers were fabricated using polyurethane with engineered soft segments as the matrix, which also exhibited capacitive sensing performance, demonstrating their multifunctional application potential.

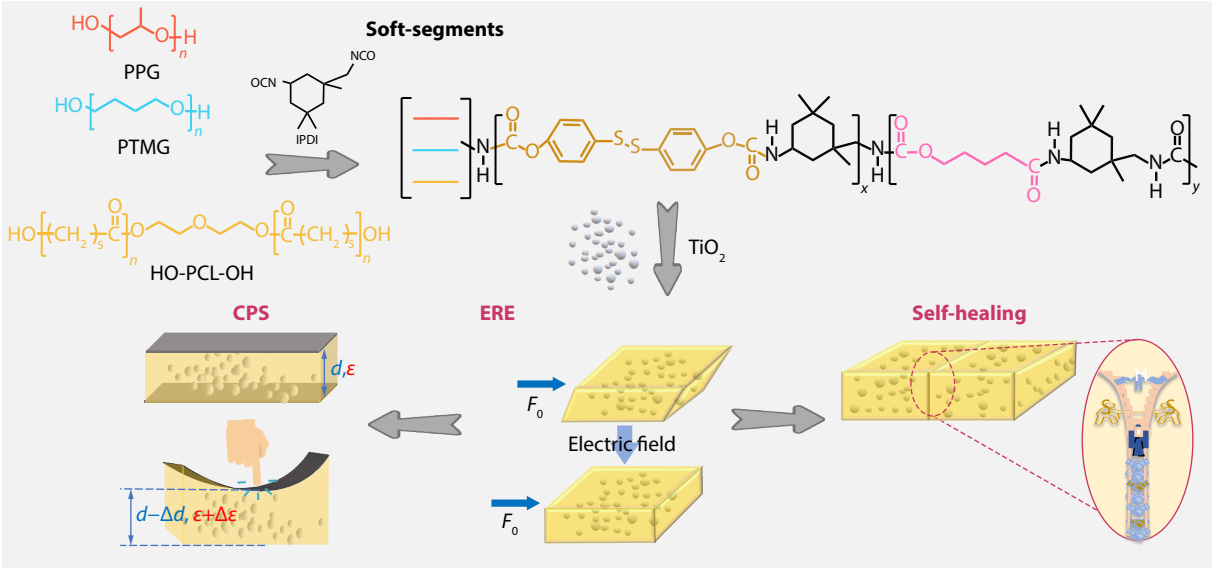

Chinese J. Polym. Sci. 2026, 44, 2269–2281 *https://doi.org/10.1007/s10118-026-3644-3*

Rheol. **2001**, *45*, 641–57.

15 Yuan, X.; Zhou, X.; Liang, Y.; Wang, L.; Chen, R.; Zhang, M.; Pu, H.; Xuan, S.; Wu, J.; Wen, W. A stable high-performance isotropic electrorheological elastomer towards controllable and reversible circular motion. *Compos. Pt. B-Eng.* **2020**, *193*, 107988.

16 Dong, X. F.; Niu, C. G.; Qi, M. Enhancement of electrorheological performance of electrorheological elastomers by improving TiO2 particles/silicon rubber interface. *J. Mater. Chem. C* **2016**, *4*, 6806–6815.

17 Xue, H.; Xu, C.; Qiu, Z.; Jiang, B.; Xiong, X. Investigation of the mechanisms by which silicone oil affects the properties of electrorheological elastomer. *J. Appl. Polym. Sci.* **2025**, *142*, e57007.

18 Zhao, Z.; Chen, Z.; Liang, Y.; Liu, Y. D.; Choi, H. J. Polydimethylsiloxane-based polyurethane as the matrix of electrorheological elastomers with an adjustable dielectric constant and improved field-active efficiency. *ACS Appl. Polym. Mater.* **2023**, *5*, 10363–10372.

19 Wu, S.; Ma, S.; Zhang, Q.; Yang, C. A comprehensive review of polyurethane: properties, applications and future perspectives. *Polymer* **2025**, *327*, 128361.

20 Huyan, C.; Liu, D.; Han, X.; Liu, D.; Li, H.; Tsui, O. K. C.; Su, L.; Qin, X.; Pan, C.; Chen, F.; Zhang, L. Delayed crystallization response-inspired waterborne polyurethane with high performance. *Nat. Commun.* **2025**, *16*, 9546.

21 Luo, H.; Deng, H.; Zhu, Y.; Shi, H.; Zhang, C.; Wang, Y. High-performance polyurethane elastomers with mechano-responsive self-reinforcing via rigid-flexible segments regulation. *Compos. Pt. B-Eng.* **2025**, *297*, 112287.

22 Qin, J.; Chen, Y.; Guo, X.; Huang, Y.; Chen, G.; Zhang, Q.; He, G.; Zhu, S.; Ruan, X.; Zhu, H. Regulation of hard segment cluster structures for high-performance poly(urethane-urea) elastomers. *Adv. Sci.* **2024**, *11*, 2400255.

23 Liu, B.; Niu, Z.; Wang, Z.; Wang, Y.; Zou, H.; Zhao, X.; Hu, S. Effect of hard segment content on the phase separation and properties of hydroxyl-terminated polybutadiene thermoplastic polyurethane. *Polym. Test.* **2025**, *143*, 108681.

24 Akindoyo, J. O.; Beg, M. D. H.; Ghazali, S.; Islam, M. R.; Jeyaratnam, N.; Yuvaraj, A. R. Polyurethane types, synthesis and applications – a review. *RSC Adv.* **2016**, *6*, 114453–114482.

25 Tian, J.; Zhou, Z.; Miao, X.; Wang, S.; Ming, Y.; Nie, Y.; Ma, Y.; Li, Z. Supertough, resilient, and healable thermoplastic poly(urethane urea) elastomers by dense packing of hydrogen-bonding arrays. *Adv. Funct. Mater.* **2026**, *36*, e04882.

26 Fu, Y.; Zhang, S.; Li, B.; Wang, L.; Zhang, Y.; Ye, Z.; Zhou, Y.; Yi, J.; Qin, H.; Shi, Q.; Yang, Q.; Wang, S.; Xiong, C.; Nie, S.; Wang, Q.

Highly ordered rubbers with a giant elastocaloric effect. *Sci. Adv.* **2026**, *12*, eady2745.
27 Mei, X.; Lu, W.; Dong, J. R.; Pan, K. H.; Tan, J. J.; Yan, H. Y.; Wu, J.; Zhou, Y.; Chen, H. X. Influence of soft segment length on the dielectric polarization behavior of ketal-containing polyurethane elastomer. *Chinese J. Polym. Sci.* **2026**, *44*, 189–197.
28 Zhao, Z. H.; Zhu, S. F.; Li, B.; Niu, C. G.; Tong, Y.; Ma, N.; Dong, X. F.; Han, B. G.; Huang, H.; Qi, M. A Stiffness tunable self-healing composite comprising pdms and titanium dioxide. *ACS Appl. Polym. Mater.* **2022**, *4*, 2656–2663.
29 Xu, H.; Tu, J.; Li, H.; Ji, J.; Liang, L.; Tian, J.; Guo, X. Room-temperature self-healing, high ductility, recyclable polyurethane elastomer fabricated via asymmetric dynamic hard segments strategy combined with self-cleaning function application. *Chem. Eng. J.* **2023**, *454*, 140101.
30 Luo, Y.; Chen, J.; Situ, G.; Li, C.; Zhang, C.; Li, F.; Li, C. H.; Luo, Z.; Zhang, X. Aromatic disulfide-induced self-reinforcing polyurethane elastomer with self-healability. *Chem. Eng. J.* **2023**, *469*, 143958.
31 Li, Y.; Zhou, M.; Xia, L.; Yang, X.; Shi, Y. Room-temperature self-healing polyurethane elastomers with high strength and superior self-healing efficiency based on aromatic disulfide-induced. *Colloid Surf. A-Physicochem. Eng. Asp.* **2024**, *681*, 132829.
32 He, Y.; Xie, D.; Zhang, X. The structure, microphase-separated morphology, and property of polyurethanes and polyureas. *J. Mater. Sci.* **2014**, *49*, 7339–7352.
33 Yamamoto, T.; Shibayama, M.; Nomura, S. Structure and properties of fatigued segmented poly(urethaneurea)s iii. quantitative analyses of hydrogen bond. *Polym. J.* **1989**, *21*, 895–903.
34 Zhang, H.; Zhang, F.; Wu, Y. Robust stretchable thermoplastic polyurethanes with long soft segments and steric semisymmetric hard segments. *Ind. Eng. Chem. Res.* **2020**, *59*, 4483–4492.
35 Wu, G. ; Song, X. ; Yang, Z. ; Li, Y. ; Zhang, H. Synthesis and characterization of biodegradable polyester/polyether wpu as the environmental protection coating. *J. Polym. Environ.* **2022**, *30*, 528–540.
36 Zhao, X.; Niu, C.; Jia, Z.; Dong, X.; Xiong, X. Magnetic field-enhanced anisotropic electrorheological elastomer with magnetic/electric dual-responsive rod particles. *Polym. Compos.* **2025**, *46*, 6755–6767.
37 Kwon, S. H.; Lee, C. J.; Choi, H. J.; Chung, K. H.; Jung, J. H. Viscoelastic and mechanical behaviors of magneto-rheological carbonyl iron/natural rubber composites with magnetic iron oxide nanoparticle. *Smart Mater. Struct.* **2019**, *28*, 045012.
38 Khan, W. I.; Zhang, Z.; Yousaf, M.; Ma, N.; Dong, X. Exploring the potential of induced dipole-dominated electrorheological effect: advancing ER elastomers. *Smart Mater. Struct.* **2024**, *33*, 125001.
39 Xiang, D.; Liu, M.; Chen, G. L.; Zhang, T.; Liu, L.; Liang, Y. R. Optimization of mechanical and dielectric properties of poly(urethane urea)-based dielectric elastomers via the control of microstructure. *RSC Adv.* **2017**, *7*, 55610–55619.
40 Yang, X. Y.; Liu, S. S.; Korobko, A. V.; Picken, S. J.; Besseling, N. A. M. Changes of the molecular mobility of poly(ε-caprolactone) upon drawing, studied by dielectric relaxation spectroscopy. *Chinese J. Polym. Sci.* **2018**, *36*, 665–674.
41 Zhao, Z.; Chen, Z.; Zhang, M.; Liang, Y.; Choi, H. J.; Liu, Y. D. The effect of particle surface modification on electric-field-induced modulus control and actuation strain of polyurethane/TiO2 elastomers. *Colloid Surf. A-Physicochem. Eng. Asp.* **2025**, *710*, 136280.
42 Mathew, S.; Chintagumpala, K. A review of recent progress in flexible capacitance pressure sensors: materials design, printing methods, and applications. *Adv. Compos. Hybrid Mater.* **2025**, *8*, 236.
43 Li, T.; Fang, X.; Pang, Q.; Huang, W.; Sun, J. Healable and shape editable supercapacitors based on shape memory polyurethanes. *J. Mater. Chem. A* **2019**, *7*, 17456–17465.

https://doi.org/10.1007/s10118-026-3644-3